Biomedical Signal Processing and Control 112 (2026) 108440

Contents lists available at ScienceDirect

Biomedical Signal Processing and Control

journal homepage: www.elsevier.com/locate/bspc

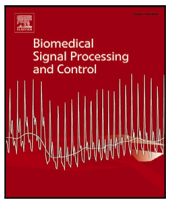

A quantum-inspired medical scalable convolutional neural network for Intelligent pneumonia diagnosis

Dongfen Li, Yuchen Sun *, Yuhang Yuan, Zhikang Hu, Qiuyu Xiang, Yangyang Jiang, Yonghao Zhu, You Fu, Xiaoyu Hua

College of Computer Science and Cyber Security (Pilot Software College), Chengdu University of Technology, Erxianqiao East Third Road, Chengdu, 610059, China

ARTICLE INFO

Keywords:
Quantum deep learning
Quantum computing
Artificial intelligence
Medical image processing
Convolutional neural network

ABSTRACT

Biomedical images play a crucial role in clinical diagnosis, patient detection and management. Traditional medical image classification methods usually rely on manual feature extraction, which is difficult to capture complex image features. Moreover, some traditional algorithms are computationally inefficient and have long processing time when dealing with large-scale medical image data. Given the limitations of traditional methods, deep learning, especially convolutional neural networks (CNNs), has become a powerful tool for modern medical image classification. By automatically learning image features, convolutional neural networks can significantly improve the classification accuracy and efficiently process complex medical image data. Despite the excellent performance of convolutional neural networks in medical image classification, their computational resource requirements are still high. To address this problem, we propose a novel model, a quantum-inspired medical scalable convolutional neural network (MSQCNN). The MSQCNN system consists of a number of small-scale quantum devices to achieve full utilization of quantum resources and alleviate the present-day difficulty of preparing large quantum computers. We train this network on an image dataset containing chest radiographs and benchmark its performance. Compared with other benchmark models, our model performs even better. MSQCNN not only achieves an average accuracy of 97.71% on the test set, but also obtains an F1-score of 98.46%, an AUC value of 99.47%, a recall of 98.43%, and a precision of 98.50%. Moreover, we conclude that MSQCNN models have excellent resilience to noise by numerical simulations.

1. Introduction

A novel coronavirus, Severe Acute Respiratory Syndrome Coronavirus 2 (SARS-CoV-2), was first identified in December 2019 as the causative agent of a respiratory disease that has been named coronavirus disease 2019, or Covid-19 [1]. First reported in December 2019 in Wuhan, Hubei Province, China, the subsequent outbreak rapidly spread from local to global, creating one of the most serious global public health crises of the 21st century [2,3]. The outbreak affected several aspects, especially the public health system [4–6]. As an important aid in the detection of novel coronavirus pneumonia, computed tomography (CT) images and X-ray images can present the characteristics of the lung infection, making it easy for physicians to recognize the effects of novel coronavirus on the lungs. With the development of technology, the demand for intelligent medical diagnostic systems is increasing, and there are higher requirements for realizing efficient and accurate biomedical image classification.

Traditional biomedical image classification usually relies on manual feature extraction and classical machine learning algorithms [7]. However, because of the huge amount of medical image data and complex features, the efficiency of relying on traditional methods to process images is very low, and the adaptability is poor. Modern biomedical image classification techniques mainly rely on deep learning, especially convolutional neural networks and their variants [8,9]. As a subfield of machine learning, deep learning is more prominent in both the complexity of the network structure and the automation of feature extraction. Deep learning algorithms are capable of automatically extracting image features from data without manual intervention [10,11]. In recent years, 3D CNN-based models [12], Deep Residual Networks (ResNet) [13], Generative Adversarial Networks (GAN) [14], etc. have further improved classification performance. More complex models such as multimodal models can also combine different types of medical image information, such as CT and MRI, to provide more comprehensive classification results. Recent studies have applied a variety of innovative approaches in the field of medical image analysis: [15]

* Corresponding author.
E-mail address: sunyuchen@stu.cdut.edu.cn (Y. Sun).

https://doi.org/10.1016/j.bspc.2025.108440
Received 11 November 2024; Received in revised form 5 July 2025; Accepted 1 August 2025
Available online 30 August 2025

used the ResNet-50 deep learning model for colon cancer cell (HT-29) detection; [16] combined hybrid segmentation and digital breast tomosynthesis (DBT) for breast cancer classification; and [17] applied the Modified Artificial Bee Colony Algorithm (M-ABC) and K-nearest neighbor (KNN) to optimize feature selection for heart disease prediction. These research results not only show the great potential of deep learning in medical image analysis, but also provide an important reference for our research.

However, the problem faced by deep learning is that it has too many learning model parameters, which require high data volume and computational resources. Meanwhile, the proposal of quantum deep learning provides a new solution to solve traditional machine learning tasks. Quantum computing utilizes qubits to process information in parallel and is able to achieve exponential acceleration in theory. The ability to extract features can be improved through the superposition and entanglement properties of quanta. However, quantum deep learning is currently in the preliminary stage of development, and it is very difficult to prepare large quantum computers with many qubits.

In this paper, we present a scalable quantum convolutional neural network, MSQCNN, for medical image classification. The MSQCNN system consists of multiple small quantum devices. It combines classical devices and quantum computing, achieving fewer parameters. Since many biomedical images are non-public, we chose to apply the model on Chest X-ray Images (Pneumonia) and ChestMNIST datasets. Experiments were performed on PennyLane and PyTorch. The experimental results show that our proposed model is feasible and has better performance. The contributions of this paper are summarized as follows.

- A scalable Multi-Small Quantum Convolutional Neural Network (MSQCNN) is proposed for biomedical image classification, which addresses the quantum resource limitations in the NISQ era by decomposing complex classification tasks into parallel subtasks processable by multiple small quantum devices, thereby providing a practical quantum-assisted approach for medical image analysis under current technological constraints.
- The experimental results validate the excellent performance of MSQCNN in pneumonia diagnosis, with an accuracy of 97.71%, which is much better than traditional neural networks. What is more, the experiments demonstrate that the model performance significantly improves with the increase of quantum resources, which provides a clear performance improvement path for future quantum hardware development.
- Regarding the noise resistance of the proposed method, the experimental results show that under 1% and 10% depolarization noise environments, the MSQCNN model still maintains excellent performance compared to the ideal noise-free situation, fully verifying that the method has good noise robustness.

The rest of this paper is structured as follows: Section 2 reviews the related work and analyzes the limitations of the existing research, Section 3 introduces the theoretical foundations of quantum computation, quantum deep learning, and parameterized quantum circuits, Section 4 elaborates on the architectural design and workflow of the MSQCNN model, Section 5 verifies the validity and superiority of the model through experiments, Section 6 summarizes the main contributions, and Section 7 looks forward to future research directions.

2. Literature review

2.1. Related works

Wu et al. [18] proposed the UIU-Net (U-Net in U-Net) framework that effectively solves the problems of target loss and feature discriminative limitation caused by the increase of network depth in traditional methods when dealing with small targets through the nested U-Net structure. The framework performs well in infrared small-target detection, and its multi-scale feature extraction and local global context information fusion strategies are inspiring for small-target detection in medical image classification, especially in challenging scenarios such as low-contrast, complex backgrounds or small-size lesions.

Li et al. [19] proposed the LRR-Net that combines a low-rank representation (LRR) model with deep learning techniques to efficiently solve the LRR model using an ADMM optimizer and incorporate the solution as a priori knowledge into a deep network to guide parameter optimization. The method performs well in hyperspectral anomaly detection, and its multi-scale feature extraction and local global contextual information fusion strategy significantly improves the model's ability to detect small targets.

Houssein et al. [20] proposed the hybrid quantum–classical convolutional neural network (HQ-CNN) model that combines the advantages of quantum computing and classical convolutional neural networks, utilizing randomized quantum circuits (RQCs) as a quantum convolutional layer to process the image data to extract complex features. Experiments show that HQ-CNN outperforms traditional CNN models on small-scale datasets with shorter training time, providing a new solution for medical image classification.

Hassan et al. [21] proposed a model combining quantum convolutional neural network (QCNN) and ResNet(50) for classifying MNIST medical datasets. The model achieves a classification accuracy of 99.6% on the MNIST dataset, which outperforms the model using QCNN or ResNet(50) alone, demonstrating the potential of quantum computing in medical image classification.

Li et al. [22] proposed a method based on a classical-to-quantum (CQ) integration model combining deep learning and quantum computing techniques for diagnosing COVID-19 via chest CT images. The method utilizes pre-trained ResNet50, VGG16, and AlexNet networks to extract features, and uses quantum circuits as classifiers, showing high classification accuracy and robustness.

Arora et al. [23] proposed the MLDC model that combines deep learning and quantum computing techniques to classify multi-class lung diseases by artificial neural network (ANN) and quantum classifier (QC). The experimental results show that the MLDC-QC model achieves an accuracy of 97.5% on the multi-class lung disease dataset, demonstrating high classification accuracy and efficiency.

Martis et al. [24] proposed a lung cancer detection method based on a hybrid quantum architecture that combines deep learning and quantum computing techniques using chest X-ray and computed tomography images. The system achieved 92.12% accuracy and 94% sensitivity, demonstrating the potential of quantum computing in medical image analysis.

Sengupta and Srivastava [25] proposed a quantum neural network (QNN)-based medical image classification method for fast diagnosis of COVID-19 patients. The QNN model runs on quantum-optimized hardware in 52 min, which is 30 min faster than conventional GPU hardware, and has an accuracy that is 2.92% higher than 2D CNNs, with an average recall of 97.7%.

Amin et al. [26] proposed a quantum machine learning (QML)-based COVID-19 classification method to improve classification accuracy by generating synthetic data through conditional generative adversarial network (CGAN). The QML model outperforms classical machine learning models on both datasets (UCSD-AI4H/COVID-CT and POF Hospital), reaching maximum accuracy of 96% and 100%, respectively.

Oviesi et al. [27] proposed a quantum neural network-assisted learning method for small medical datasets, specifically targeting the detection of emphysema. This hybrid quantum–classical neural network model combines quantum variational circuits with CNNs, and the generalization ability of the model in data-limited situations is improved through pre-training and fine-tuning. The experimental results show that the quantum-assisted model outperforms the traditional CNN model in both accuracy and F1-score, with an accuracy of 0.5690 and an F1-score of 0.5990.

2.2. Limitations and challenges

Although deep learning and quantum computing have made significant progress in the field of medical image classification in recent years, there are still some limitations and unresolved issues in existing research, and these gaps provide new directions and opportunities for our research. Although classical methods such as UIU-Net [18] and LRR-Net [19] have made progress in multi-scale feature extraction and small target detection, they still face the challenge of computational inefficiency when dealing with large-scale datasets. Current quantum–classical hybrid models, including HQ-CNN [20], QCNN-ResNet combinations [21], and classical-quantum integration approaches [22], have demonstrated encouraging results but fail to address the fundamental quantum hardware scalability problem, which relies on single large-scale quantum circuits, which is impractical in the current NISQ era. Furthermore, models such as MLDC [23], hybrid quantum architectures for lung cancer detection [24], and QNN-based COVID-19 classification [25] still require a large number of classical parameters and quantum components, failing to take full advantage of the quantum parallelism that significantly reduce the number of parameters.

Furthermore, existing quantum methods exhibit inconsistent performance, lack clinical interpretability, and have accuracy rates ranging from modest improvements in the case of small datasets [27] to high, but potentially overfitting results [21,26]. Most importantly, current quantum medical image classification models, including those proposed by Martis et al. [24], Sengupta and Srivastava [25], Amin et al. [26], treat medical images as generalized data, do not consider clinical diagnostic workflows and do not provide region-specific feature extraction consistent with radiographic practices. These models also lack robust strategies for effectively utilizing multiple small-scale quantum devices in parallel, limiting their practical deployment in clinical environments with limited quantum hardware resources. Given the limited exploration of quantum architectures specifically designed to utilize unique qua ntum properties (superposition, entanglement, quantum parallelism) for capturing subtle pathological features in medical imaging, MSQCNN aims to address this challenge through its innovative multi-scale quantum convolutional approach and parallel quantum feature extractor.

To explore this potential, this paper proposes a novel quantum-inspired medical scalable convolutional neural network (MSQCNN) that efficiently utilizes quantum resources through multiple small quantum devices. The MSQCNN improves computational efficiency and reduces hardware requirements while demonstrating strong generalization ability and diagnostic accuracy on medium-sized datasets, achieving an average accuracy of 97.71% on the test set. Additionally, the model enhances the extraction of complex image features by leveraging quantum computing principles. These contributions offer a promising approach for medical image classification with potential for broader applications.

3. Theoretical background

3.1. Quantum gates

A quantum computer consists of wires and elementary quantum gates that describe, in the language of quantum computing, changes in quantum states that are caused by a series of unitary operations. The most basic fundamental operations are quantum logic gates, which are reversible, which is what distinguishes them from classical logic gates. Quantum logic gates are also known as qubit gates, and the basic qubit gates are categorized into two types according to the number of qubits involved: single-qubit gates and two-qubit gates.

Single-qubit gates mainly consist of Pauli gates (I, X, Y, Z) and Hadamard gates. The matrix of Pauli gates can be expressed as:

$$X = \begin{pmatrix} 0 & 1 \\ 1 & 0 \end{pmatrix}, Y = \begin{pmatrix} 0 & -i \\ i & 0 \end{pmatrix}, Z = \begin{pmatrix} 1 & 0 \\ 0 & -1 \end{pmatrix} \quad (1)$$

The X-gate acts equivalently to the NOT-gate on a classical computer, flipping the quantum state; the Y-gate rotates the arrow on the Bloch sphere by an angle π around the Y-axis; and the Z-gate acts by being able to rotate the arrow on the Bloch sphere by an angle π around the Z-axis. The H-gate can be expressed as $H = \frac{1}{\sqrt{2}}\begin{pmatrix} 1 & \\ 1 & -1 \end{pmatrix}$, which transforms $|0\rangle$ into $\frac{|0\rangle+|1\rangle}{\sqrt{2}}$, and transforms $|1\rangle$ to $\frac{|0\rangle-|1\rangle}{\sqrt{2}}$.

A rotation gate is a parameterized gate for rotating the state of a qubit on a Bloch sphere:

$$R_X(\theta) = \cos(\theta/2)I - i\sin(\theta/2)X, \quad (2)$$

$$R_Y(\theta) = \cos(\theta/2)I - i\sin(\theta/2)Y, \quad (3)$$

$$R_Z(\theta) = \cos(\theta/2)I - i\sin(\theta/2)Z \quad (4)$$

These quantum gates offer distinct advantages for medical image processing applications. Parameterized rotation gates (RY and RZ) provide continuous parameter spaces that are essential for gradient-based optimization in machine learning tasks. Unlike discrete gates, rotation gates enable fine-tuned feature extraction through their adjustable angles, making them particularly suitable for capturing subtle variations in medical imaging data. The controlled-RZ (CRZ) gate creates quantum entanglement between qubits while maintaining relatively low hardware complexity compared to multi-qubit gates, making it practical for implementation on current NISQ devices. This combination of parameterized single-qubit gates and controlled two-qubit gates provides an optimal balance between expressive power and hardware feasibility for medical image classification tasks.

3.2. Quantum Deep Learning (QDL)

Quantum deep learning (QDL) is an emerging research field that combines quantum computing and deep learning. Compared with traditional deep learning models, quantum neural network (QNN) utilizes the principle of state superposition, which has a speed advantage in processing high-dimensional data, and can achieve exponential acceleration of learning ability and processing speed. Its basic process is to encode traditional data into quantum data, go through quantum information processing, and finally obtain the computational results through measurement, as shown in Fig. 1.

QDL has shown promising applications in several fields. In medical image classification, Landman et al. [28] and Ajlouni et al. [29] proposed quantum-assisted neural networks and quantum–classical hybrid models, respectively, confirming the potential of quantum methods. In finance, the QENN scheme was used to predict stock closing prices [30]. In materials science, the quantum graph neural network proposed by Ryu et al. [31] converges faster and with lower loss than classical models in predicting molecular properties.

Although QDL faces challenges such as immature quantum hardware, complex algorithm design, and quantum–classical integration, research has made significant progress. The quantum convolutional neural network (QCNN) proposed by Cong et al. [32] requires only O(log(N)) variational parameters, which makes it suitable for near-term quantum devices. Pesah et al. [33] demonstrated that the QCNN does not suffer from the problem of vanishing gradients, which provides real-world applications with theoretical support. Overall, quantum deep learning, as an emerging technology that combines the strengths of two major fields, shows great potential despite the challenges.

3.3. Parameterized Quantum Circuit (PQC)

A parameterized quantum circuit (PQC), also known as a variational quantum circuit (VQC), is a type of quantum circuit consisting of a series of quantum gate operations, each of which contains adjustable parameters. These parameters allow fine-tuning of the circuit's operations to suit different computational tasks, thereby exploring and optimizing multiple properties of quantum systems.

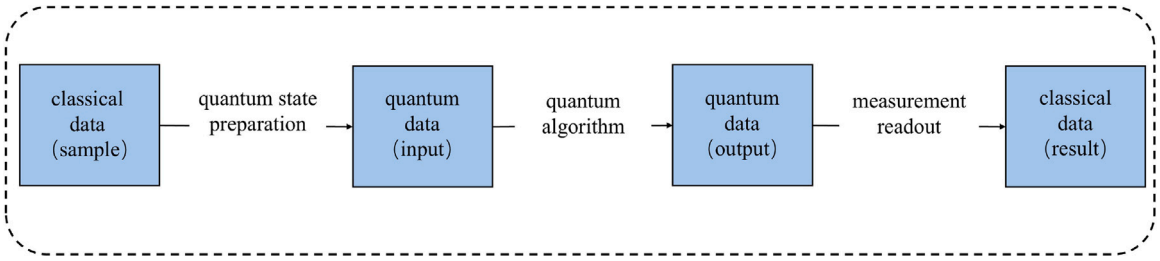

Fig. 1. The basic process of quantum deep learning. Classical data is encoded into quantum data, which undergoes a series of operations to get the final output.

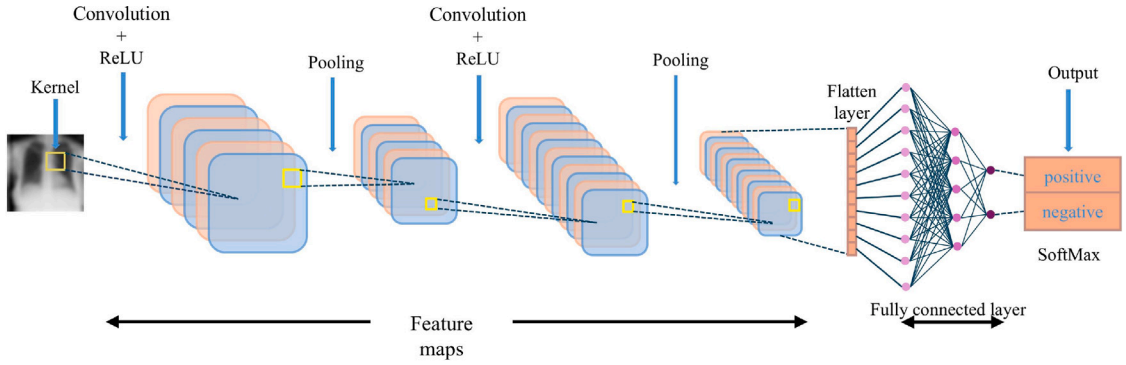

Fig. 2. Structure of a classical convolutional neural network. The whole process from input to output of classification results for the task of categorizing chest radiographs as an example.

A PQC typically consists of three key components: a parameterized quantum circuit, a loss function, and a classical optimizer. The core of a PQC contains a set of quantum gates with adjustable parameters, such as rotation gates (RX, RY, and RZ gates), where the parameters control the angle of rotation of these gates. The parameters are represented as a vector and are continuously adjusted by the classical optimizer during iterations to minimize the loss function. The loss function is used to quantify the difference between the output result of the circuit and the desired value, while the classical optimizer optimizes the parameter configuration by minimizing the loss function.

4. Methodology

4.1. Classical model

A classical convolutional neural network consists of the following components: convolutional layer, activation function, pooling layer, fully connected layer and output layer. In addition, CNNs contain some auxiliary components, such as Batch Normalization and Dropout layers, to help optimize the model performance. The specific model architecture is shown in Fig. 2.

In a neural network, the input layer is the first layer of the neural network and is responsible for receiving data from external inputs. These data can be images, sounds, text, sensor data, etc. The main role of the input layer is to pass this data to the network in the form of numerical values for subsequent processing and analysis. Taking an image as an example, the input data is passed through the convolutional layer, which performs a convolutional operation to extract features. The convolution kernel is slid over the input image and the result obtained is:

$$S(i,j) = (X * W)(i,j) = \sum_{m=0}^{M-1} \sum_{n=0}^{N-1} X(i+m, j+n) \cdot W(m,n) \tag{5}$$

where $X(i,j)$ denotes the value of the input and $W(m,n)$ denotes the weight matrix of the convolution kernel. Sometimes the original future map edges are also patched with zeros, such an operation is useful because the edges of the image should also be filled with features, a process known as zero padding. The convolution operation is the key to the first layer of a convolutional network, which is like the retina of a human being, preprocessing the image at first sight of the image before it is handed over to the brain. The output of the convolutional layer is also usually passed through a nonlinear activation function, common activation functions include ReLU, which can be expressed as $A(i,j) = \mathrm{ReLU}(S(i,j)) = \max(0, S(i,j))$, which introduces a nonlinear property by setting negative values in the convolutional result to 0 and retaining positive values. The pooling layer follows the convolutional layer and performs downsampling operations on the feature maps output from the convolutional layer, and the pooling operation is mainly to reduce the dimensionality of the feature maps. The result finally passes through the fully connected layer, which integrates the global features of the input data through its fully connected nature and further maps these features to the output layer for the final classification or regression task. After training the neural network on a large amount of data, the parameters are optimized to find the minimum value of the loss function.

4.2. MSQCNN model

Our model incorporates quantum computing technology on the basis of traditional convolutional neural networks and proposes a scalable quantum convolutional neural network model for medical diagnosis, taking into account the limited availability of large-scale quantum computing devices in the NISQ era. Quantum computing not only reduces computation time, but also improves the accuracy of extracted features for recognition. The MSQCNN model breaks away from the traditional design idea of quantum neural networks and adopts a new parallel modular architecture. Unlike the traditional approach that requires the complete image to be processed on a single quantum device, our innovation lies in partitioning the image into multiple sub-regions to be processed simultaneously by multiple small quantum devices, which not only solves the practical problem of the current limitations of the scale of quantum hardware, but also improves the parallel efficiency of the feature extraction. This architectural design represents an important paradigm shift in quantum medical image processing, making

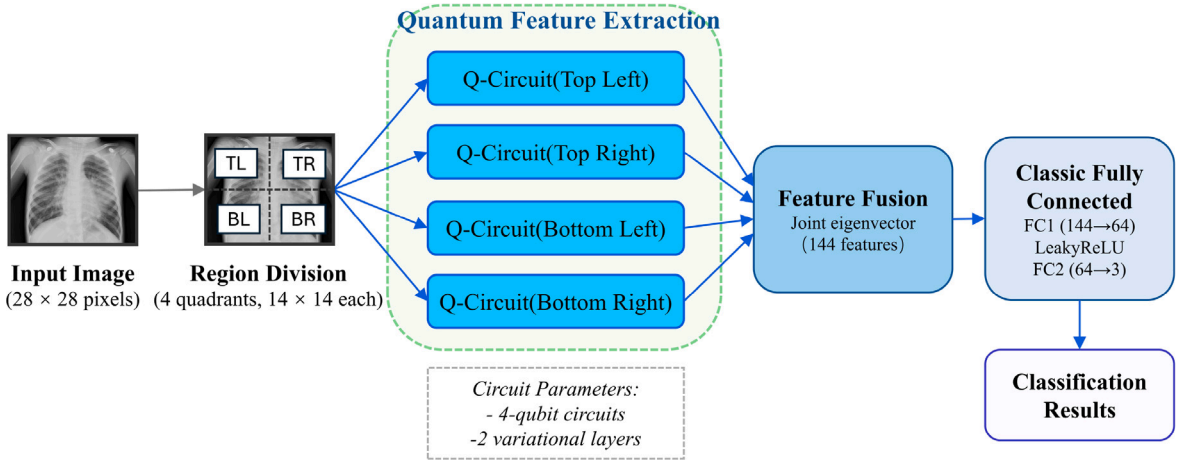

Fig. 3. Overall structure of the 16-qubit MSQCNN model. The MSQCNN model consists of four parallel quantum feature extractors and one classical classifier. The input 28 × 28 pixel medical image is divided into four 14 × 14 equal-sized blocks, which are processed by independent quantum feature extractors. The features produced by each quantum feature extractor are merged and fed into the classical classifier to generate the final classification result.

quantum advantage no longer limited to theoretical possibilities, but an achievable goal under current technological conditions.

The idea is that originally there were a number of small-scale quantum devices in the system, and we used several of them as feature extractors to extract image features, after which the extracted features were fed into the classical fully-connected layer for final classification. Several of the feature extraction devices are run in parallel. This has the advantage of alleviating the present situation of limited quantum resources and putting these devices to good use. Suppose there are m quantum devices in the system. We divide the input image into m blocks of equal size and feed them into m quantum devices, which have the same initial parameters and circuit structure. After a series of operations, the features of the corresponding part of the image are obtained. The overall architecture of the model is shown in Fig. 3.

Our proposed MSQCNN is a hybrid quantum–classical network architecture that achieves efficient medical image classification through multiple parallel quantum devices. The model first divides the 28 × 28-pixel input image $\mathbf{X} \in \mathbb{R}^{28\times28}$ into four 14 × 14 blocks $\{\mathbf{X}_{TL}, \mathbf{X}_{TR}, \mathbf{X}_{BL}, \mathbf{X}_{BR}\} \in \mathbb{R}^{14\times14}$, each of which is processed by an independent quantum feature extractor. Each quantum feature extractor is based on a parameterized quantum circuit and contains three key components: the initialization layer uses Hadamard gates to place the four qubits in superposition state; the data encoding layer uses alternating RZ and RY rotation gates to encode the classical state $\{x_i\}$ into the quantum state $|\psi_{\text{input}}\rangle$ through angle encoding, which is selected over amplitude encoding due to its superior noise resilience and simpler hardware implementation on NISQ devices; and the variational layer contains two layers of quantum gate operations, each layer first uses the CRZ gates to create quantum entanglement between neighboring qubits (forming a ring topology), where CRZ gates are chosen to provide parameterized entanglement control that enables fine-tuned quantum correlations essential for medical pattern recognition, and then applies RY gates for single-bit rotations; the rotation angles of these gates are the trainable parameters. Finally, the expectation value of each qubit is obtained as a feature by Pauli-Z measurement $\langle Z_j\rangle = \langle\psi_{\text{final}}|\sigma_z^{(j)}|\psi_{\text{final}}\rangle$, where $|\psi_{\text{final}}\rangle = U(\boldsymbol{\theta})|\psi_{\text{input}}\rangle$. This circuit design fully utilizes quantum entanglement and superposition properties to capture complex feature patterns that are difficult to extract by conventional convolution. The alternating RZ-RY encoding sequence ensures comprehensive Bloch sphere coverage, maximizing the encoding expressivity, while the ring topology of CRZ gates ensures balanced connectivity without requiring long-range interactions that are challenging for current quantum hardware. The principle used to realize the quantum convolution operation is shown in Fig. 4.

The parameter optimization of the model adopts a hybrid quantum–classical training method, which utilizes the PennyLane framework to achieve seamless integration of quantum circuits with PyTorch. Taking the 16-qubit model as an example, each quantum feature extractor contains 16 trainable parameters (2 layers × 8 parameters/layer), which are updated by backpropagation and the Adagrad optimizer, with the parameter updating rule as $\theta^{(t+1)} = \theta^{(t)} - \eta\nabla\theta\mathcal{L}(\theta^{(t)})$, where η is the learning rate and $\mathcal{L}$ is the cross-entropy loss function. For the input image block $\mathbf{X}_i$, the feature extraction process can be represented as a sliding window operation:

$$\mathbf{f}_i = \Phi_Q(\mathbf{X}_i;\boldsymbol{\theta}_i) = \{[\langle Z_0\rangle_{w,h}, \langle Z_1\rangle_{w,h}, \langle Z_2\rangle_{w,h}, \langle Z_3\rangle_{w,h}] | w,h \in \mathcal{W}\} \tag{6}$$

where W denotes the set of all sliding window positions. The outputs of the four feature extractors are combined as $\mathbf{F} = [\mathbf{f}_{TL}, \mathbf{f}_{TR}, \mathbf{f}_{BL}, \mathbf{f}_{BR}] \in \mathbb{R}^{576}$. After feature extraction, the classical fully-connected network is responsible for the final classification decision, resulting in a hybrid quantum–classical architecture that combines the advantages of quantum computing in feature extraction with the efficiency of classical neural networks in dealing with high-dimensional features. Experimental results show that this hybrid architecture achieves superior classification performance while maintaining low resource requirements.

The present model has significant computational advantages in theory. From the perspective of quantum resource utilization, the small quantum device in our 16-qubit model uses 4 qubits and 2 layers of variational circuit structure, each containing a coding layer (Hadamard gates to create superposition states, RZ/RY gates for angle coding) and a variational layer (CRZ gates to create entanglement, RY gates to parameterize operations). Each quantum feature extractor contains 16 trainable parameters (2 layers × 8 parameters/layer), and the four parallel quantum convolutional layers use a total of 64 quantum parameters. The circuit depth is $O(n_{\text{layers}})$, and the quadrant image processing strategy splits the 28 × 28 image into four 14 × 14 subregions for parallel processing, significantly reducing the input complexity of a single quantum circuit. With the development of dedicated quantum processors, the quantum advantages of MSQCNN in processing complex medical images will become more significant [34,35]. The MSQCNN architecture demonstrates scalability across different input image resolutions. When using 28 × 28 pixel images, the quantum circuit architecture remains consistent for larger inputs (e.g., 100 × 100 pixels). For larger images, each 50 × 50-pixel block requires adjustment of the convolution parameters (kernel size and stride) to ensure that the feature dimension is compatible with the number of qubits in the quantum feature extractor. By selecting an appropriate kernel size, the quantum encoding complexity remains constant, while the variational circuit structure and optimization strategy remain unchanged.

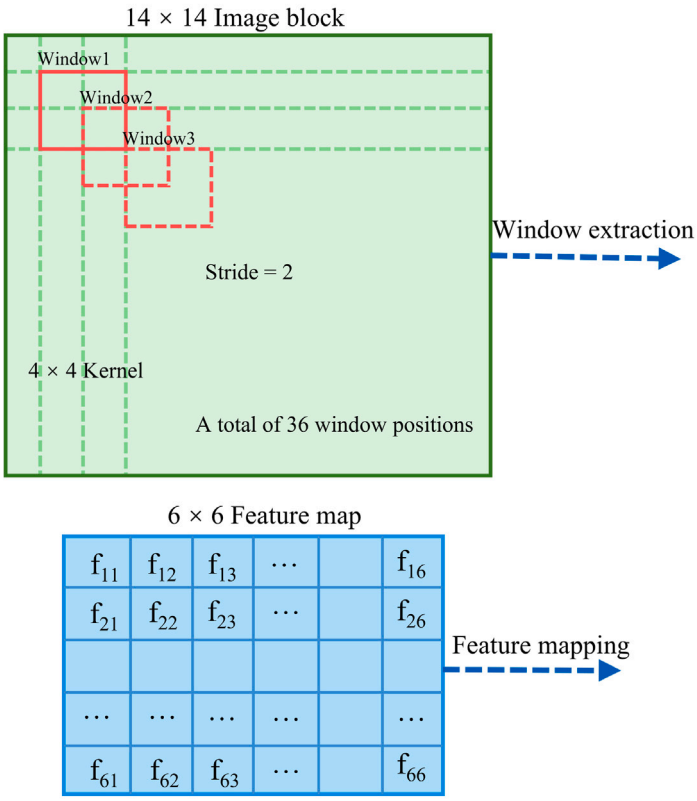

(a) Quantum convolutional sliding window processing

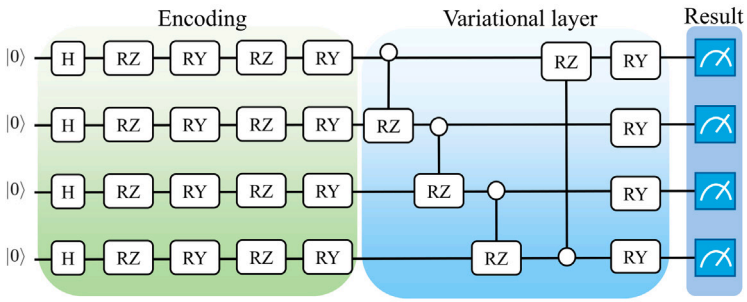

(b) Detailed structure diagram of quantum feature extractor circuit

Fig. 4. Principle of quantum convolution operation implementation. (a) Quantum convolution sliding window processing. (b) Detailed architecture of the quantum feature extractor circuit. It contains the initialization layer, the data encoding layer encodes the classical state into a quantum state using angle encoding, the variational layer contains quantum gates with trainable parameters, and finally the measurements are obtained by Pauli-Z measurements.

4.3. Workflow

In this section, we describe the workflow of the whole system, as shown in Fig. 5. Take the classification task on the Chest X-ray Images dataset as an example. First, the system loads the Pneumonia X-ray Images dataset, which contains images of both normal and pneumonia categories. The X-ray images in the dataset are preprocessed by adjusting the original images to grayscale images of 28 × 28 pixels and normalizing them. In order to improve the generalization ability of the model, to prevent overfitting, and to evaluate the performance of the model, we divided the dataset into training, validation, and test sets in the ratio of 7:1:2. After obtaining the processed data, the system employs a four-segmentation processing strategy to uniformly segment each 28 × 28 input image into four 14 × 14 subregions. Each subregion is independently fed into the corresponding feature extractor for parallel processing, and the respective local features are extracted by quantum convolution operation.

For the quantum coding part, we use an angle coding method to encode classical data into quantum states. A Hadamard gate is first applied to the qubits to create a superposition state, and then the image data is encoded into a quantum circuit via RZ and RY rotation gates. Compared to other coding methods, angle coding is more straightforward and simpler to implement, and quantum circuits are less expensive to realize.

The encoded quantum states are passed through a variational quantum circuit for feature extraction. The quantum circuit contains an entanglement layer and a parameterized rotation layer, and the data features are learned through entanglement between quantum gates and

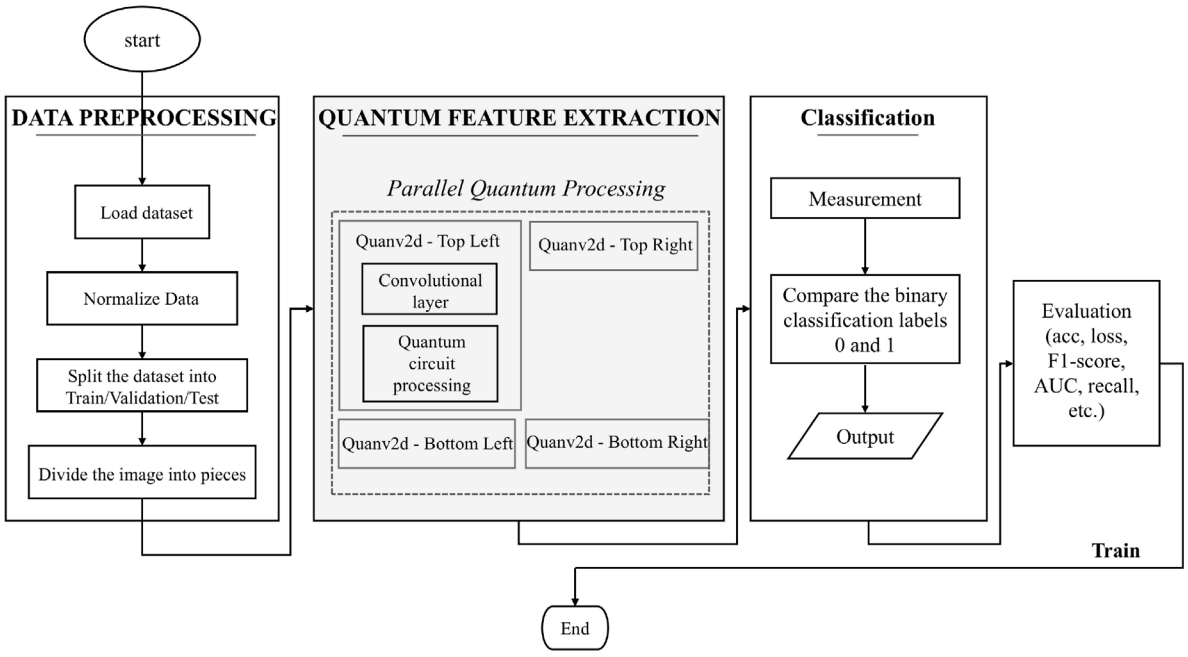

Fig. 5. Workflow of the MSQCNN. The process includes data preprocessing, feature extraction using quantum devices, classification, and evaluation stages to obtain the final results.

other quantum operations. We do not need to additionally use a ReLU-like activation function to introduce nonlinearities to the quantum convolutional layer because the quantum operations themselves have natural nonlinear properties.

Measurements are made on the quantum circuits, and local quantum features are obtained by computing the expectation values via the Pauli-Z operator. The four output features are converted to one-dimensional feature vectors and spliced. The feature vectors are then passed through a fully connected layer to obtain the final classification output. During the training process, the model parameters are optimized using the cross-entropy loss function and the Adagrad optimizer. The gradient computation employs PennyLane's parameter-shift rule for quantum parameters, which calculates the gradient of a parameterized quantum gate U(θ) as $\frac{\partial\langle\psi(\theta)|H|\psi(\theta)\rangle}{\partial\theta} = \frac{1}{2}\left[\left\langle\psi\left(\theta+\frac{\pi}{2}\right)|H|\psi\left(\theta+\frac{\pi}{2}\right)\right\rangle - \left\langle\psi\left(\theta-\frac{\pi}{2}\right)|H|\psi\left(\theta-\frac{\pi}{2}\right)\right\rangle\right]$. This analytical differentiation approach requires two circuit evaluations per parameter with phase shifts of $\pm\frac{\pi}{2}$, specifically applied to the variational layer parameters containing both controlled-RZ entangling gates and single-qubit RY rotation gates with parameter tensor shape $(n\_layers, 2\times n\_qubits)$. The quantum gradients integrate seamlessly with PyTorch's automatic differentiation framework through the TorchLayer wrapper interface (diff_method='best'), enabling end-to-end backpropagation and simultaneous optimization of both quantum circuit parameters and classical neural network weights via standard gradient descent. Several evaluation metrics are monitored in real time during the training process, including accuracy, loss, F1-score, AUC, and recall. The core of backpropagation is the chain rule, which implements the gradient computation of quantum parameters through the parameter offset rule, and the weights of each layer are updated by gradient descent. Several evaluation metrics are monitored in real time during the training process, including accuracy, loss, F1-score, AUC, and recall.

MSQCNN demonstrates strong clinical alignment through its four parallel quantum feature extractors that process distinct image regions, closely mirroring radiologists' standardized diagnostic workflow. This architecture corresponds well to the systematic approach radiologists employ when reading chest radiographs — methodically examining the upper left lung field, upper right lung field, lower left lung field, and lower right lung field, searching for lesion signs region by region. This correspondence between the model's technical design and established clinical practice facilitates potential integration into existing diagnostic workflows as a clinical decision support tool.

5. Experiments and results

To evaluate the effectiveness and reliability of the MSQCNN model, we conducted a series of experiments using two datasets. The results of these experiments show that our approach outperforms other network models in terms of classification performance and exhibits good scalability. In the following sections, we provide a comprehensive overview of the datasets used, the evaluation metrics employed, and the experimental setting. Subsequently, we will present our experimental results on all datasets, including a series of ablation studies, in order to provide a comprehensive analysis of the performance of our model.

5.1. Data description and pre-process

Due to the privacy-preserving needs of visiting patients and the scarcity of quantum computing resources, we chose two datasets that are publicly available to be downloaded.

Chest X-ray Images (Pneumonia): This dataset is a chest X-ray image dataset for pneumonia detection and contains 5863 chest X-ray images categorized into "pneumonia" and "normal". The "normal" category contains 1587 images and the "pneumonia" category contains 4276 images. The dataset was divided into a training set, a test set, and a validation set for model training and evaluation. All images were initially normalized to a uniform size of 1857 × 1317 pixels, but were rescaled to a grayscale image of 28 × 28 pixels during the data preprocessing stage. The image files were organized into two categories, normal and pneumonia, converted to PyTorch tensors and then spread to one-dimensional vectors and multiplied by 2π for scale transformation, while the normal sample labels were coded as 0 and the pneumonia samples were coded as 1. This preprocessing scheme effectively reduces the dimensionality of the image data while retaining the key features required for diagnosis, providing standardized training data for the pneumonia diagnostic model.

ChestMNIST: The ChestMNIST dataset was constructed based on the NIH-ChestXray14 dataset containing 112,120 frontal radiographic images of 30,805 unique patients and image labels of 14 diseases

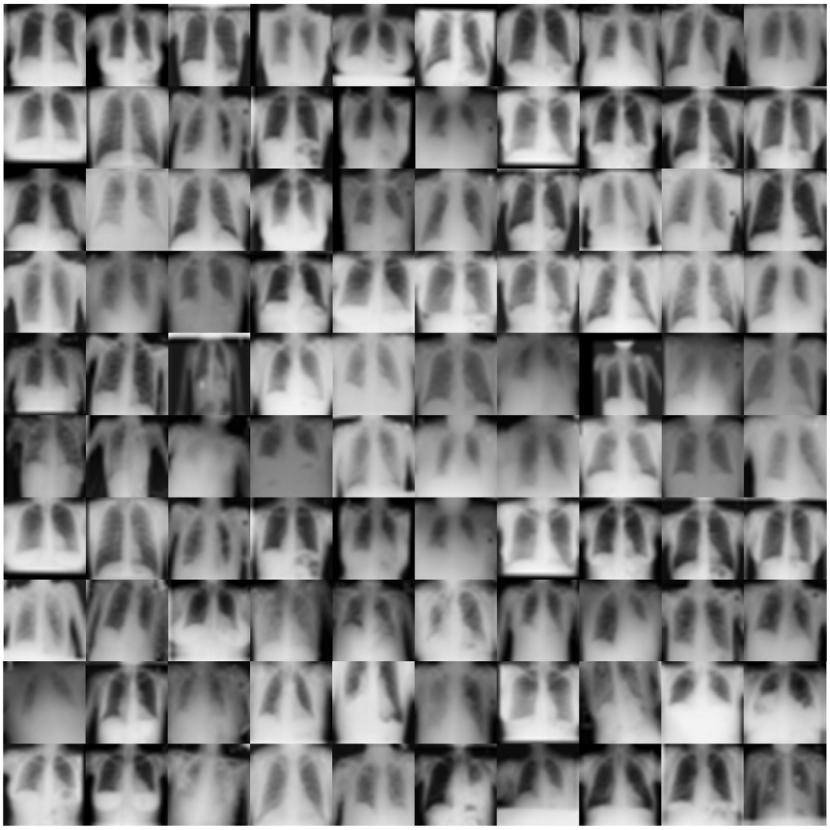

Fig. 6. Visualization of dataset samples. It contains 50 negative and 50 positive samples.

obtained through text mining, which can be formulated as a multi-label binary classification task (see Fig. 6).

The dataset was resized from 1 × 1024 × 1024 to 1 × 100 × 100 using the official data partitioning of the source images. In MedMNIST, ChestMNIST was partitioned into 78,468 training images, 11,219 validation images and 22,433 test images. We performed dichotomous classification, categorizing images as normal and non-normal.

Subsequently, the samples were divided into several equal-sized parts according to the needs of the model. This prepares them for feeding into the quantum circuit for subsequent processing. Assume that there are $m + 1$ devices in the system and m are used for feature extraction. Since the quantum devices in the system cannot load instances that are too large, the instance x is divided into m small chunks, which can be represented as $\{x_1, x_2, \ldots, x_m\}$. As an example, a 16-qubit MSQCNN system consists of four small-scale HQCNNs, where the input image is 100 × 100 and is divided into four 50 × 50 segments.

5.2. Evaluation metrics and implementation

In this study, we employ a comprehensive set of evaluation metrics to critically assess the performance of the proposed model. These include core performance metrics such as accuracy, precision, recall, and F1-score [36], each of which provides unique insights on classification performance from different perspectives. Accuracy measures the proportion of correctly categorized instances across all predictions, providing a measure of the overall effectiveness of the model. It is calculated by Eq. (7):

$$\text{Accuracy} = \frac{TP + TN}{TP + TN + FP + FN} \tag{7}$$

where TP is true positive, TN is true negative, FP is false positive, and FN is false negative.

Precision measures the proportion of categories predicted to be positive that are actually positive, reflecting the model's ability to avoid false positives. In medical scenarios such as pneumonia diagnosis, false positives may lead to unnecessary treatments and patient anxiety, thus the precision is important for clinical decision making [37]. As shown in Eq. (8):

$$\text{Precision} = \frac{TP}{TP + FP} \tag{8}$$

This indicator is particularly important for assessing the reliability of the model in positive predictions.

Recall measures the proportion of actual positive instances correctly identified by the model, indicating the model's ability to identify positive instances, as shown in Eq. (9):

$$\text{Recall} = \frac{TP}{TP + FN} \tag{9}$$

In applications such as medicine and risk detection, high recall is often a prioritized goal.

The F1-score is a reconciled average of precision and recall, providing a balanced metric that is particularly applicable to data with unbalanced categories, as shown in Eq. (10):

$$\text{F1} = 2 \cdot \frac{\text{Precision} \cdot \text{Recall}}{\text{Precision} + \text{Recall}} = \frac{2TP}{2TP + FP + FN} \tag{10}$$

Specificity measures the ability of a model to correctly identify negative instances and is a key indicator of avoiding false positives. In clinical practice, specificity directly affects the false-positive rate, and high specificity means that healthy individuals are less likely to be incorrectly diagnosed with a disease, which is important for avoiding unnecessary medical interventions and reducing healthcare costs [38]. Calculated from Eq. (11):

$$\text{Specificity} = \frac{TN}{TN + FP} \tag{11}$$

Specificity is an important dimension to assess in applications where the rate of false positives needs to be controlled.

Table 1
Parameters of the classifiers.

Methods	Parameters values
CNN	epochs = 20 batch_size = 16 kernel = 4 activation = LeakyReLU
DenseNet121 [39]	epochs = 20 batch_size = 16 activation = Softmax optimizer = Adam
Improved ResNet-18 [40]	epochs = 20 batch_size = 16 activation = LeakyReLU optimizer = Adam
Proposed MSQCNN	epochs = 20 batch_size = 16 kernel = 4 activation = LeakyReLU optimizer = Adagrad loss = CrossEntropyLoss

AUC is a composite measure of the performance of a dichotomous model, which is equivalent to the probability that a randomly selected positive instance is ranked higher than a randomly selected negative instance, as shown in Eq. (12):

$$\mathrm{AUC} = \int_0^1 TPR\left(FPR^{-1}(x)\right) dx \tag{12}$$

where TPR is the true-positive rate and FPR is the false-positive rate (equal to 1 - specificity). AUC values range from 0 to 1, where 1 indicates perfect categorization and 0.5 indicates random categorization. Eq. (12) calculates the area under the ROC curve, and as a single numerical metric, the AUC provides an overall assessment of the model's ability to discriminate and is not affected by category imbalance.

Our model is implemented on the CUDA 10.1 platform using the frameworks of PyTorch and PennyLane. PyTorch provides flexible tensor computation and automatic differentiation capabilities, while PennyLane is a Python library designed for quantum machine learning that seamlessly integrates classical machine learning with quantum computation. PennyLane's most notable feature is the ability to automatically compute the gradient of a quantum circuit, which makes it particularly suitable for training parameterized quantum circuits. We used Python as the main programming language, combined with NumPy for data preprocessing, with the learning rate set to 0.05 and batch size 16.

5.3. Experimental results

The model was experimented on both datasets taking the same hyperparameters to compare the generalization ability of the model and the relevant values have been listed in Table 1.

5.3.1. Performance evaluation on the chest X-ray images

The experimental results of the model on the Chest X-ray Images dataset are shown in Fig. 7. In order to comprehensively evaluate the feature extraction performance of MSQCNN, we analyze it in comparison with benchmark models such as classical CNN, DenseNet121, and Improved ResNet-18, and the relevant results are summarized in Table 2. The table shows in detail the performance of each model on two key metrics: accuracy and loss rate. Based on the comparative analysis results in Table 2, we can draw the following conclusions: the proposed MSQCNN demonstrates significant performance advantages in the image feature extraction task, achieving an accuracy rate of 0.9512 and a loss rate of 0.1553 when using 16 qubits, further improving the accuracy rate to 0.9693 and decreasing the loss rate to 0.1184 at 24 qubits, and achieving an accuracy rate of 0.9771 and a loss rate of 0.0943 at 32 qubits. The configuration achieves the best performance with an accuracy of 0.9771 and a loss rate of only 0.0943, which outperforms the comparison models in both accuracy and loss control. To evaluate the performance of MSQCNN more comprehensively, we also consider other evaluation metrics. The AUC value of 32-qubit MSQCNN is 99.47%, the value of F1-score is 98.46%, the value of recall is 98.43%, the value of precision is 98.50%, and the value of specificity is 95.63%. The results in Table 3 further confirm that with the gradual increase of quantum resources, the performance of MSQCNN shows a continuous improvement trend in all the evaluated indices, which fully verifies the positive effect of quantum computing resources on improving model performance.

Table 2
Performance comparison of different methods on the Chest X-ray Images dataset. The table shows the accuracy and loss values for classical methods (CNN, DenseNet121, Improved ResNet-18) and the proposed MSQCNN with different numbers of qubits (16, 24, 32). Bold values indicate the best results for each metric, demonstrating the superior performance of MSQCNN with 32 qubits.

Methods	Qubits	Accuracy	Loss
CNN	–	0.9159	0.2189
DenseNet121 [39]	–	0.8832	0.2845
Improved ResNet-18 [40]	–	0.9103	0.2958
MSQCNN	16	0.9512	0.1553
	24	0.9693	0.1184
	32	0.9771	0.0943

Table 3
Comprehensive performance evaluation of the MSQCNN model.

Methods	Evaluation metrics (%)				
	AUC	F1-score	Recall	Precision	Specificity
MSQCNN-16qubit	99.24	97.94	97.96	97.91	93.95
MSQCNN-24qubit	99.19	98.07	98.29	97.85	93.72
MSQCNN-32qubit	99.47	98.46	98.43	98.50	95.63

Table 4
Performance comparison on the ChestMNIST dataset. Results show accuracy and loss for classical methods (CNN, DenseNet121, Improved ResNet-18) and MSQCNN with varying qubit numbers (16, 24, 32). Bold values indicate best performance.

Methods	Qubits	Accuracy	Loss
CNN	–	0.9087	0.3012
DenseNet121 [39]	–	0.8806	0.2915
Improved ResNet-18 [40]	–	0.9016	0.3107
MSQCNN	16	0.9277	0.5913
	24	0.9599	0.4345
	32	0.9821	0.2399

Table 5
Comprehensive performance evaluation of the MSQCNN model.

Methods	Evaluation metrics (%)				
	AUC	F1-score	Recall	Precision	Specificity
MSQCNN-16qubit	95.27	92.81	92.82	92.56	95.80
MSQCNN-24qubit	97.81	95.72	95.71	95.71	97.22
MSQCNN-32qubit	98.13	97.85	97.83	97.78	98.41

5.3.2. Performance evaluation on the ChestMNIST

As shown in Table 4 and Table 5, the performance of MSQCNN model proposed in this paper is superior to the other three models compared. The MSQCNN model predicts cases with an accuracy of 0.9821, a loss rate of 0.2399, an AUC value of 98.13%, an F1-score of 97.85%, a recall of 97.83%, a precision of 97.78%, and a specificity value of 98.41%. As shown in Fig. 8, the 32-qubit MSQCNN model has the best performance in terms of average accuracy and loss rate on the test set, which also verifies that the performance of the model improves with the expansion of quantum resources.

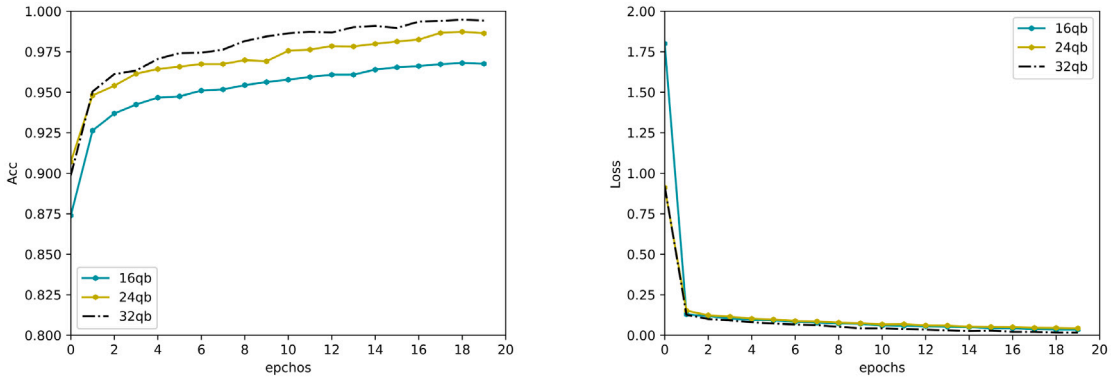

(a) Test accuracy (b) Test loss

Fig. 7. Learning curve visualization of (a) Test accuracy and (b) Test loss on the Chest X-ray Images dataset for different scales of MSQCNN models with 20 epochs.

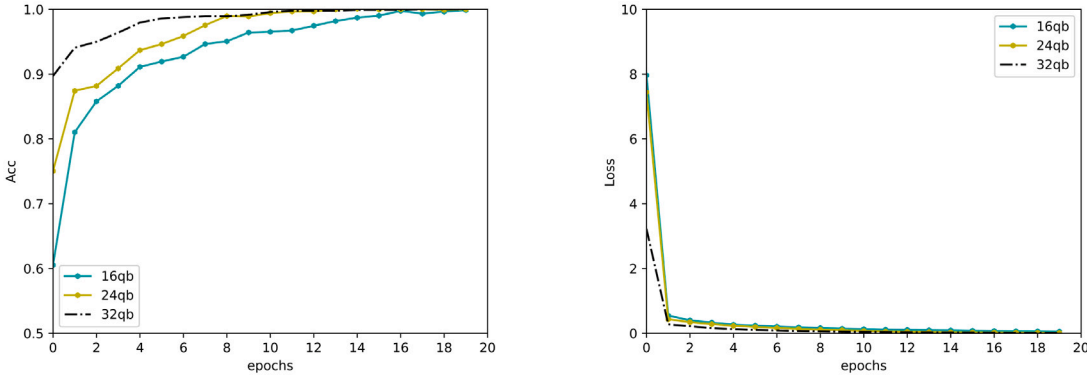

(a) Test accuracy (b) Test loss

Fig. 8. Learning curve visualization of (a) Test accuracy and (b) Test loss on the ChestMNIST dataset for different scales of MSQCNN models with 20 epochs.

5.3.3. Resilience to noise

In order to evaluate the robustness and noise immunity of MSQCNN models in real quantum computing environments, we conduct a comprehensive experimental study under different depolarizing noise conditions. Quantum systems are inherently susceptible to environmental decoherence and operational defects, making noise immunity a key performance metric for practical quantum machine learning applications. In this section, we systematically evaluate the performance of the model under three different noise levels: no-noise conditions (p=0), low-noise environments (p=0.01), and moderately noisy scenarios (p=0.1), where p denotes the probability of depolarizing noise. The depolarizing noise model is described by a completely positive trace preserving mapping $\mathcal{E}_p(\rho) = (1-p)\rho + \frac{p}{2}I$, where ρ is the single qubit density matrix and I is the unit matrix. The depolarizing noise model simulates the most common form of quantum decoherence, where the quantum state decays randomly with probability p into a maximally mixed state. We quantify the model's ability to maintain performance as the noise intensity increases, using classification accuracy as the primary evaluation metric. This analysis provides important insights into the potential of MSQCNN for practical deployment in Noisy Intermediate-Scale Quantum (NISQ) devices, where noise mitigation and fault tolerance are important considerations for realizing quantum advantages. The relevant experimental results are shown in Table 6 and Fig. 9.

Table 6
Relative impact of depolarizing noise on the classification test accuracy and loss over Chest X-ray Images dataset.

Noise level	Accuracy	Loss
0	0.9512	0.1553
1%	0.9502	0.1564
10%	0.9497	0.1595

6. Conclusion

In this paper, a medical scalable quantum convolutional neural network (MSQCNN) is proposed, which innovatively employs multiple small quantum devices to process medical images in parallel. In the pneumonia diagnosis task, the MSQCNN model achieves 97.71% accuracy, 98.46% F1-score, and 98.43% recall, which significantly outperforms traditional quantum neural networks and demonstrates good noise robustness. Experiments demonstrate that MSQCNN effectively solves the problem of limited quantum resources by decomposing complex tasks into parallelizable subtasks, providing a feasible technical path for quantum-assisted medical image analysis. The modular architecture demonstrates robustness to hardware heterogeneity through four independent quantum feature extractors, enabling seamless integration of devices with different qubit counts and capabilities. As shown in Table 6, the system maintains 94.97% accuracy under 10% depolarizing noise, demonstrating excellent noise tolerance across different quantum devices. The architecture supports scalable parameter configurations, allowing devices with varying capacities to employ deeper variational circuits while maintaining compatibility within the same deployment. This architecture not only has practical value in the current NISQ era, but also opens up a new direction for quantum applications in medical image processing. A summary of all abbreviations used in this article and their full forms is provided in Table 7.

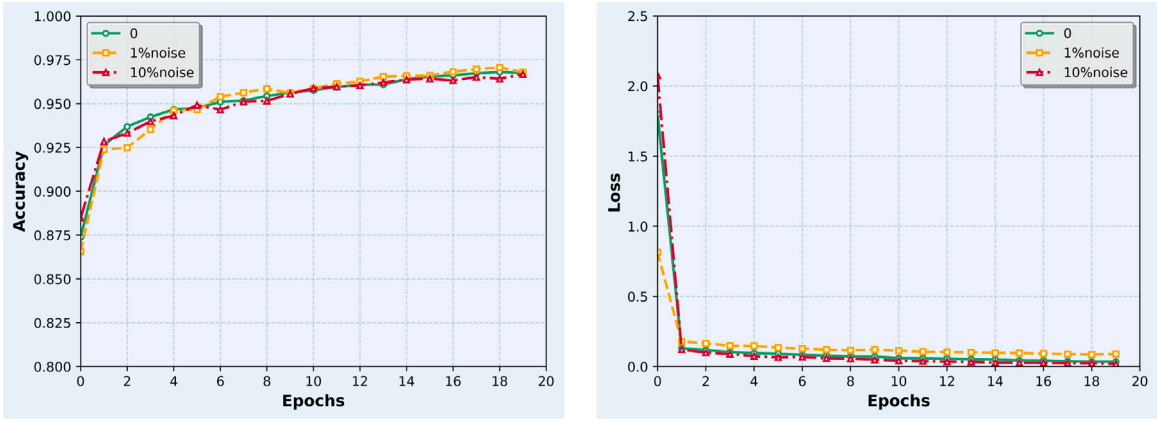

(a) Test accuracy (b) Test loss

Fig. 9. Illustration shows the relative impact of the MSQCNN method by depolarizing noise in the Chest X-ray Images dataset. In both figures, p = 0, p = 1%, and p = 10% are indicated by orange, green, blue, and red lines, respectively. (a) The relative impact of noise on the classification test accuracy. (b) The relative effect of noise on the classification test error.

7. Future work

Despite the remarkable results of this study in pneumonia diagnosis, there is still important research space in quantum device security. As MSQCNN models rely on multiple small quantum devices to process medical image data in parallel, it becomes particularly important to ensure the security of data exchange between these devices and patient data privacy protection. Future work will explore security protocols applicable to the collaborative environment of multiple quantum devices and investigate how to prevent leakage of sensitive medical data during feature extraction and classification.

Our ultimate goal is to extend the value of MSQCNN in a broader range of medical applications. Of particular interest is optimizing the model to identify small changes in the early stages of disease to improve early screening. In addition, we plan to explore the development of MSQCNN as a fusion system capable of simultaneously processing multiple medical data types (e.g., images, medical record text, and genomic data) to provide more comprehensive support for precision medicine decision making.

CRediT authorship contribution statement

Dongfen Li: Writing – review & editing, Funding acquisition, Conceptualization. **Yuchen Sun:** Writing – original draft, Validation, Methodology, Investigation, Formal analysis, Data curation, Conceptualization. **Yuhang Yuan:** Data curation, Conceptualization. **Zhikang Hu:** Investigation, Formal analysis. **Qiuyu Xiang:** Data curation, Conceptualization. **Yangyang Jiang:** Validation. **Yonghao Zhu:** Conceptualization. **You Fu:** Formal analysis. **Xiaoyu Hua:** Validation, Resources.

Funding

This work was supported in part by the National Natural Science Foundation of China (Grant Nos: 62172060), National Key R&D Program of China (Grant Nos: 2022YFB3304303), Sichuan Province Science and Technology Plan, China (24JBGS0007), Chengdu Bamo Technology Co., Ltd., China (AH2025-0099) and Sichuan Lingke Automobile Manufacturing Co., Ltd., China (AH2025-0062).

Declaration of competing interest

The authors declare that they have no known competing financial interests or personal relationships that could have appeared to influence the work reported in this paper.

Table 7
List of abbreviations.

Abbreviation	Full form
MSQCNN	Quantum-Inspired Medical Scalable Convolutional Neural Network
CNN	Convolutional Neural Network
CT	Computed Tomography
ResNet	Residual Network
GAN	Generative Adversarial Network
MRI	Magnetic Resonance Imaging
UIU-Net	U-Net in U-Net
LRR	Low-Rank Representation
HQ-CNN	Hybrid Quantum-Classical Convolutional Neural Network
RQCs	Random Quantum Circuits
QCNN	Quantum Convolutional Neural Network
CQ	Classical-Quantum
QNN	Quantum Neural Network
QML	Quantum Machine Learning
CGAN	Conditional Generative Adversarial Network
MQCNN	Medical Quantum Convolutional Neural Network
MLDC	Multi-Lung Disease Classification
QDL	Quantum Deep Learning
QENN	Quantum Elman Neural Network
QGNN	Quantum Graph Neural Network
PQC	Parameterized Quantum Circuit
VQC	Variational Quantum Circuit
SGD	Stochastic Gradient Descent
acc	accuracy
TP	True Positive
TN	True Negative
FP	False Positive
FN	False Negative
AUC	Area Under the Curve
ROC	Receiver Operating Characteristic
NISQ	Noisy Intermediate-Scale Quantum

Data availability

Data will be made available on request.

References

[1] J.H. Beigel, K.M. Tomashek, L.E. Dodd, A.K. Mehta, B.S. Zingman, A.C. Kalil, E. Hohmann, H.Y. Chu, A. Luetkemeyer, S. Kline, et al., Remdesivir for the treatment of Covid-19, N. Engl. J. Med. 383 (19) (2020) 1813–1826.

[2] C. Huang, Y. Wang, X. Li, L. Ren, J. Zhao, Y. Hu, L. Zhang, G. Fan, J. Xu, X. Gu, et al., Clinical features of patients infected with 2019 novel coronavirus in Wuhan, China, Lancet 395 (10223) (2020) 497–506.

[3] J. Zhang, M. Litvinova, W. Wang, Y. Wang, X. Deng, X. Chen, M. Li, W. Zheng, L. Yi, X. Chen, et al., Evolving epidemiology and transmission dynamics

of coronavirus disease 2019 outside Hubei province, China: a descriptive and modelling study, Lancet Infect. Dis. 20 (7) (2020) 793–802.
[4] J. Bedford, J. Farrar, C. Ihekweazu, G. Kang, M. Koopmans, J. Nkengasong, A new twenty-first century science for effective epidemic response, Nature 575 (7781) (2019) 130–136.
[5] D.E. Bloom, D. Cadarette, Infectious disease threats in the twenty-first century: strengthening the global response, Front. Immunol. 10 (2019) 549.
[6] S.I. Mallah, O.K. Ghorab, S. Al-Salmi, O.S. Abdellatif, T. Tharmaratnam, M.A. Iskandar, J.A.N. Sefen, P. Sidhu, B. Atallah, R. El-Lababidi, et al., COVID-19: breaking down a global health crisis, Ann. Clin. Microbiol. Antimicrob. 20 (1) (2021) 35.
[7] C. Cao, F. Liu, H. Tan, D. Song, W. Shu, W. Li, Y. Zhou, X. Bo, Z. Xie, Deep learning and its applications in biomedicine, Genom. Proteom. Bioinform. 16 (1) (2018) 17–32.
[8] X. Liu, L. Song, S. Liu, Y. Zhang, A review of deep-learning-based medical image segmentation methods, Sustainability 13 (3) (2021) 1224.
[9] S.M. Anwar, M. Majid, A. Qayyum, M. Awais, M. Alnowami, M.K. Khan, Medical image analysis using convolutional neural networks: a review, J. Med. Syst. 42 (2018) 1–13.
[10] N. Dhungel, G. Carneiro, A.P. Bradley, A deep learning approach for the analysis of masses in mammograms with minimal user intervention, Med. Image Anal. 37 (2017) 114–128.
[11] R. Archana, P.E. Jeevaraj, Deep learning models for digital image processing: a review, Artif. Intell. Rev. 57 (1) (2024) 11.
[12] T. Mhathesh, J. Andrew, K. Martin Sagayam, L. Henesey, A 3D convolutional neural network for bacterial image classification, in: Intelligence in Big Data Technologies—beyond the Hype: Proceedings of ICBDCC 2019, Springer, 2021, pp. 419–431.
[13] D. Sarwinda, R.H. Paradisa, A. Bustamam, P. Anggia, Deep learning in image classification using residual network (ResNet) variants for detection of colorectal cancer, Procedia Comput. Sci. 179 (2021) 423–431.
[14] J.J. Jeong, A. Tariq, T. Adejumo, H. Trivedi, J.W. Gichoya, I. Banerjee, Systematic review of generative adversarial networks (GANs) for medical image classification and segmentation, J. Digit. Imaging 35 (2) (2022) 137–152.
[15] I. Haq, T. Mazhar, R.N. Asif, Y.Y. Ghadi, R. Saleem, F. Mallek, H. Hamam, A deep learning approach for the detection and counting of colon cancer cells (HT-29 cells) bunches and impurities, PeerJ Comput. Sci. 9 (2023) e1651.
[16] W.M. Idress, K.A. Abouda, R. Javed, M. Aoun, Y.Y. Ghadi, T. Shahzad, T. Mazhar, A.M. Ibrahim, Hybrid segmentation and 3D imaging: Comprehensive framework for breast cancer patient segmentation and classification based on digital breast tomosynthesis, Biomed. Signal Process. Control. 100 (2025) 106992.
[17] M.A. Khan, T. Mazhar, M. Mateen Yaqoob, M. Badruddin Khan, A.K. Jilani Saudagar, Y.Y. Ghadi, U.F. Khattak, M. Shahid, Optimal feature selection for heart disease prediction using modified artificial bee colony (M-ABC) and K-nearest neighbors (KNN), Sci. Rep. 14 (1) (2024) 26241.
[18] X. Wu, D. Hong, J. Chanussot, UIU-net: U-net in U-net for infrared small object detection, IEEE Trans. Image Process. 32 (2022) 364–376.
[19] C. Li, B. Zhang, D. Hong, J. Yao, J. Chanussot, LRR-net: An interpretable deep unfolding network for hyperspectral anomaly detection, IEEE Trans. Geosci. Remote Sens. 61 (2023) 1–12.
[20] E.H. Houssein, Z. Abohashima, M. Elhoseny, W.M. Mohamed, Hybrid quantum-classical convolutional neural network model for COVID-19 prediction using chest X-ray images, J. Comput. Des. Eng. 9 (2) (2022) 343–363.
[21] E. Hassan, M.S. Hossain, A. Saber, S. Elmougy, A. Ghoneim, G. Muhammad, A quantum convolutional network and ResNet (50)-based classification architecture for the MNIST medical dataset, Biomed. Signal Process. Control. 87 (2024) 105560.
[22] W. Li, X. Deng, H. Zhao, H. Shao, Y. Jiang, COVID-19 diagnosis prediction using classical-to-quantum ensemble model with transfer learning for CT scan images, Imaging Sci. J. 69 (5–8) (2021) 319–333.
[23] R. Arora, G.E. Rao, S. Banerjea, B. Rajitha, MLDC: multi-lung disease classification using quantum classifier and artificial neural networks, Neural Comput. Appl. 36 (7) (2024) 3803–3816.
[24] J.E. Martis, S. MS, A. Mutawa, M. Murugappan, Novel hybrid quantum architecture-based lung cancer detection using chest radiograph and computerized tomography images, Bioengineering 11 (8) (2024) 799.
[25] K. Sengupta, P.R. Srivastava, Quantum algorithm for quicker clinical prognostic analysis: an application and experimental study using CT scan images of COVID-19 patients, BMC Med. Inform. Decis. Mak. 21 (2021) 1–14.
[26] J. Amin, M. Sharif, N. Gul, S. Kadry, C. Chakraborty, Quantum machine learning architecture for COVID-19 classification based on synthetic data generation using conditional adversarial neural network, Cogn. Comput. 14 (5) (2022) 1677–1688.
[27] S. Oviesi, M.J. Tarokh, et al., Quantum neural network-assisted learning for small medical datasets: a case study in emphysema detection, J. Supercomput. 81 (1) (2025) 1–32.
[28] J. Landman, N. Mathur, Y.Y. Li, M. Strahm, S. Kazdaghli, A. Prakash, I. Kerenidis, Quantum methods for neural networks and application to medical image classification, Quantum 6 (2022) 881.
[29] N. Ajlouni, A. Özyavaş, M. Takaoğlu, F. Takaoğlu, F. Ajlouni, Medical image diagnosis based on adaptive hybrid quantum cnn, 2023.
[30] G. Liu, W. Ma, A quantum artificial neural network for stock closing price prediction, Inform. Sci. 598 (2022) 75–85.
[31] J.-Y. Ryu, E. Elala, J.-K.K. Rhee, Quantum graph neural network models for materials search, Materials 16 (12) (2023) 4300.
[32] I. Cong, S. Choi, M.D. Lukin, Quantum convolutional neural networks, Nat. Phys. 15 (12) (2019) 1273–1278.
[33] A. Pesah, M. Cerezo, S. Wang, T. Volkoff, A.T. Sornborger, P.J. Coles, Absence of barren plateaus in quantum convolutional neural networks, Phys. Rev. X 11 (4) (2021) 041011.
[34] T. Pattnaik, P. Kanungo, P.K. Sahoo, T. Kar, P. Jain, M.S. Soliman, M.T. Islam, An efficient low complex-functional link artificial neural network based framework for uneven light image thresholding, IEEE Access (2024).
[35] P.K. Sahoo, M.K. Panda, U. Panigrahi, G. Panda, P. Jain, M.S. Islam, M.T. Islam, An improved VGG-19 network induced enhanced feature pooling for precise moving object detection in complex video scenes, Ieee Access (2024).
[36] A. Houkan, A.K. Sahoo, S.P. Gochhayat, P.K. Sahoo, H. Liu, S.G. Khalid, P. Jain, Enhancing security in industrial IoT networks: Machine learning solutions for feature selection and reduction, IEEE Access (2024).
[37] H. Chhabra, U. Chauhan, P. Jain, L.D. Sharma, A. Dev, Machine learning assisted EEG signal classification for automated diagnosis of mental stress, in: Artificial Intelligence in Biomedical and Modern Healthcare Informatics, Elsevier, 2025, pp. 447–454.
[38] P. Jain, J. Yedukondalu, H. Chhabra, U. Chauhan, L.D. Sharma, EEG-based detection of cognitive load using VMD and LightGBM classifier, Int. J. Mach. Learn. Cybern. 15 (9) (2024) 4193–4210.
[39] R. Fan, S. Bu, Transfer-learning-based approach for the diagnosis of lung diseases from chest X-ray images, Entropy 24 (3) (2022) 313.
[40] Y. Xu, G. He, D. Chen, A ResNet based pneumonia classification algorithm for chest X-Ray images, in: 2024 IEEE 6th International Conference on Power, Intelligent Computing and Systems, ICPICS, IEEE, 2024, pp. 1588–1592.